Highly efficient antibacterial surfaces based on bacterial/cell size selective microporous supports

Nelson Vargas-Alfredo,[1] Ana Santos-Coquillat, [2] Enrique Martínez-Campos,[2] Ane Dorronsoro,[3] Aitziber L. Cortajarena,[3,4] Adolfo del Campo[5] and Juan Rodríguez-Hernández[1]*

1. Instituto de Ciencia y Tecnología de Polímeros (ICTP), Consejo Superior de Investigaciones Científicas (CSIC), C/Juan de la Cierva 3, 28006 Madrid, Spain. Email: jrodriguez@ictp.csic.es .

2. Tissue Engineering Group; Instituto de Estudios Biofuncionales(IEB). Universidad Complutense de Madrid (UCM). Paseo Juan XXIII, Nº1, 28040 Associated Unit to the ICTP-CSIC group.

3. CIC biomaGUNE, Parque Tecnológico de San Sebastián, Paseo Miramón 182, 20014 Donostia-San Sebastián, Spain

4. Ikerbasque, Basque Foundation for Science, Mª Díaz de Haro 3, 48013 Bilbao, Spain

5. Instituto de Cerámica y Vidrio (ICV-CSIC), C/Kelsen 5, 28049-Madrid, Spain.

Abstract

We report on the fabrication of efficient antibacterial substrates selective for bacteria, *i.e.* non-cytotoxic against mammalian cells. The strategy proposed is based on the different size of bacteria (1-4 μm) in comparison with mammalian cells (above 20 μm) that permit the bacteria to enter in contact with the inner part of micrometer size pores where the antimicrobial functionality has been placed. On the contrary, mammalian cells, larger in terms of size, remain at the top surface thus reducing adverse cytotoxic effects and improving the biocompatibility of the substrates. For this purpose, we fabricated well-ordered functional microporous substrates (3-5 μm) using the breath figures approach (BFs) that enabled the selective functionalization of the pore cavity while the rest of the surface remained unaffected. Microporous surfaces were prepared from polymer blends of polystyrene and either polystyrene-b-poly(dimethylaminoethyl methacrylate) (PDMAEMA) or a quaternized polystyrene-b-poly(dimethylaminoethyl methacrylate) (PDMAEMAQ). As a result, porous surfaces with narrow size distribution and a clear enrichment of the PDMAEMA or the quaternized PDMAEMA block inside the pores were obtained that, in the case of the quaternized PDMAEMA, provided excellent antimicrobial activity to the films.

Keywords

Antibacterial polymer surfaces, porous materials, PDMAEMA, quaternized, cell adhesion, Breath Figures

Introduction

One of the still remaining major issues in the use of polymeric materials, in particular for biomedical applications, is directly related with the common occurring contamination by microorganisms and, among others, by bacteria. The biomedical applications in which polymers are currently playing an important role are numerous including healthcare products, hospitals or dental equipment and medical devices. However, microorganism contamination is a general problem independently of the biomaterial and the final biomedical application considered. A clear example is the case of long-term implants, such as, long-term catheters that are generally affected by implant-associated infections and need to be replaced.[1-3] Moreover, polymers have been also employed for other purposes that require materials free of microorganisms such as water purification systems, food storage, food packaging or household sanitation.[4-5]

For this reason, multiple approaches have been developed to produce polymer interfaces with reduced/limited microbial adhesion properties. These strategies typically involve the introduction of antibacterial moieties that can be either covalently anchored at the surface or are embedded in the polymeric material and gradually released.[6] Together with the surface chemical composition, the surface structure at the micro/nanometer scale of the biomaterial appears to be equally crucial to determine the extent of microbial immobilization. As a result, micrometer roughness has been reported to favor microbial adhesion and, in particular, bacterial while nanometer scale surface patterns have been found to reduce the bacterial adhesion.[7] Thus, in order to fabricate long-term antimicrobial surfaces both chemistry and surface topography need to be integrated in the same material.

In view of the potential use in the fabrication of implants it is desirable to combine excellent antimicrobial properties with low cell damage, i.e. biocompatibility (low cytotoxicity, appropriate cell adhesion and proliferation). The fabrication of antimicrobial supports usually has associated negative effects on the cell adhesion and proliferation. As a result, it is of paramount importance to fabricate surfaces able to either selectively repel bacterial adhesion or

kill them upon contact while enabling cells to attach, proliferate and even differentiate on polymer surfaces. To the best of our knowledge, these two aspects, antimicrobial activity and biocompatibility have been, in the case of polymer surfaces, typically studied separately. Just few examples have been reported in the recent literature were both aspects have been investigated.[8-10] One of the few studies have been recently reported by Raphel *et al.*[11] that reported the fabrication of multifunctional coatings able to simultaneously promote osseointegration and prevent infection for the fabrication of orthopaedic implants.

Within this context, this contribution propose a novel strategy in order to produce efficient antimicrobial surface attempting overcome the limitations of previous designs by taken into consideration both the chemistry required at the surface level and the microstructuration simultaneously. The strategy proposed resorts to the use of the Breath Figures (BFs) approach to fabricate porous surfaces with controlled chemistry and pore sizes. This approach which involves a simple and straightforward evaporation process using a polymer solution enables the fabrication of polymeric surface with precise surface topography (pores with variable sizes 2-20 μm) and chemical distribution. For this reason, several studies have been focused on the elaboration of porous films having variable pore shapes, chemistry and even exhibiting hierarchical organization, for instance, by using block copolymers.[12-14]

Patterned polymer surfaces prepared by the BFs approach have been evaluated as supports to direct cell adhesion processes in view of their potential use for tissue engineering purposes.[15-16] More precisely, the BFs technique has been proposed as a very simple and versatile method to fabricate micropatterned cell culture substrates [16-28] but also as adhesion barriers or to reduce postoperative adhesion when using fibrinolytic agents or anticoagulants, among others. [29-30] The systems explored for bioapplications up to date have been limited to few chemically different polymeric materials such as commercially available polymers, e.g. polycaprolactone [31] or amphiphilic copolymers.[32] In addition, as it has been mentioned above, investigations that combine studies with microorganisms and cells using porous films prepared by the breath figures approach are unprecedented. Both aspects have been studied separately and only few

studies have evaluated the antimicrobial/antifouling properties of the honeycomb patterned surfaces.[30]

In this study, micrometer size porous surfaces in which the inner part of the pore is decorated with an antimicrobial polymer were fabricated. These surfaces selectively favor the contact between the antimicrobial polymer located inside of the pores and the bacteria while limiting the contact with cells. The principle of this strategy relies on the difference in size between bacteria (1-5μm) and eukaryotic cells (~20μm). It is expected that porous films with pore sizes between 3-5 μm are excellent platforms to accommodate bacteria and therefore kill them while mammalian cells with larger sizes will remain intact at the surface. As antimicrobial polymers we will employ quaternary ammonium groups obtained upon quaternization of poly(dimethylaminoethyl methacrylate) (PDMAEMA). Quaternary ammonium groups[33-35] have been already employed due to their excellent efficiency killing on contact as a result of the interaction between these groups and the negatively charged groups present in the bacterial cell wall. Moreover, in order to limit the contact between these antimicrobial groups and mammalian cells (reported also to have a net negative plasmatic membrane charge), these functional groups will be precisely placed inside of the pores thus remaining only accessible to bacteria.

Cell adhesion and growth as well as the antibacterial efficiency will be thoroughly evaluated using porous films prepared using both the non-quaternized and quaternized PDMAEMA and PS as control substrate. Previous works have been reported in the preparation of porous surfaces using this type of amphipilic block copolymers. However, two main differences can be mentioned between this and previous works. On the one hand, previous works were limited to the use of the block copolymer.[36-37] Herein we fabricated the porous films from blends of the block copolymer and the homopolymer. As will be described, this allows us to precisely control the chemical distribution of the polar functional groups. On the other hand, this manuscript focuses on the fabrication of antimicrobial and biocompatible platforms using the quaternized

form of the PDMAEMA block. To the best of our knowledge, this aspect has not been considered previously. [36, 38]

Experimental section

Materials

Styrene (S, Aldrich) and dimethylaminoethyl methacrylate (DMAEMA, AR) were purified by reduced pressure distillation to remove inhibitor. The monomers were stored at –5 °C for later use. Benzyl bromide (AR) was normally distilled and stored under an argon atmosphere at –5 °C. CuBr and 2,2'-bipyridyl were used as received without further purification. N,N,N',N'',N''-pentamethyldiethylenetriamine (PMDETA) (Aldrich, 99%), copper (I) bromide (CuBr) (Aldrich 98%), ethyl-2-bromoisobutyrate (EBrIB) and the rest of solvents were employed as received without further purification.

High molecular weight polystyrene (PS) (Aldrich, $M_w = 2.50x10^5$ g/mol) was used as polymeric matrix while tetrahydrofuran (THF), chloroform ($CHCl_3$) and carbon disulfide (CS_2) were purchased from Scharlau and employed as solvents. Round glass coverslips of 12 mm diameter were supplied from Ted Pella Inc.

Polymer synthesis

Synthesis of polystyrene macroinitiator (PS-Br)

In a typical polymerization experiment, 0.60 g (3.2 mmol) phenylethyl bromide, 0.56 g (3.2 mmol) N,N,N',N'',N''-pentamethyldiethylenetriamine and 0.46 g (3.2 mmol) CuBr were placed in a dried 100 mL three-necked flask which was flushed with nitrogen. Pre-degassed styrene (20 g, 192 mmol) was added to the flask immersed in an oil bath at 85°C, and then the solution was magnetically stirred for 4 h under a nitrogen atmosphere. Over this period the originally red translucent polymeric solution turned dark and opaque. After the polymerization was completed, the polymer was diluted by 20 mL $CHCl_3$, and then precipitated in excess methanol

after passing through an alumina column. The white powder was purified by re-dissolution in $CHCl_3$ and reprecipitation in methanol, and then dried at 60°C under vacuum.

Synthesis of polystyrene-block-poly(dimethylaminoethyl methacrylate) (PS-b-PDMAEMA)

Synthesis of block copolymer: In a Schlenk tube, 0.819 g (0.182 mmol) PS-Br macroinitiator, 0.019 g (0.135 mmol) CuBr, and 0.023 g (0.135 mmol) N,N,N',N'',N''-pentamethyldiethylenetriamine (PMDETA), 20 mL of pre-degassed DMF was introduced under nitrogen atmosphere. The Schlenk was immersed in an oil bath at 90°C and the ATRP was started by adding 2.55 g (16.2 mmol) of DMAEMA. The reaction was left for 24 h with continuous stirring. After the polymerization was completed, the former block was precipitated in methanol after passing through an alumina column, and dried at 60°C under vacuum. According to ^{1}H-NMR the block copolymer has a composition of PS_{42}-*b*-$PDMAEMA_{16}$. GPC of the block copolymers carried out in THF evidenced a narrow polydispersities between 1.22-1.26 evidencing a complete initiation of the polystyrene macroinitiator.

Quaternization of the PDMAEMA units in the block copolymers

In a round bottom flask 0.1 g ($2.33x10^{-4}$ mol of tertiary amine groups) of block copolymer PS_{42}-*b*-$PDMAEMA_{16}$ were introduced and dissolved in 1.0 mL of THF under stirring at room temperature. Next, 0.0661 g ($4.65x10^{-4}$ mol) of CH_3I was added. After 20h, the quaternized copolymer was observed in form of a white powder precipitate. After evaporation of the solvent and residual CH_3I a white powder was recovered and analyzed by ^{1}H-NMR (illustrative spectra of quaternized and non-quaternized block copolymers are included in the supporting information – Figure S1).

Characterization

Scanning electron microscopy (SEM) micrographs were taken using a Philips XL30 with an acceleration voltage of 25 kV. The samples were coated with gold-palladium (80/20) prior to scanning.

Confocal Raman Microscopy: Raman spectra and images were recorded in a Confocal Raman Microscopy WITec Alpha 300 RA (Ulm, Germany) using a Nd:YAG laser of 532 nm wavelength at 10 mW output power, through a 100X objective (N.A: 0.95) and two different gratings of 600 and 1800 grooves/line. The Raman images were taken point by point with each 100 nm with a piezodriven stage and an optical fiber of 25 microns in diameter as pinhole to guarantee a spatial resolution less than 300 nm. The software Witec Project Plus was employed to analyze the spectra and to make all the calculations and to build the Raman images.

Preparation of the honeycomb films with variable surface chemical composition.

Different blends were prepared by mixing high molecular weight polystyrene matrix (between 100 and 80 wt. %) with the appropriate block copolymer (0 and 20 wt. %), maintaining constant the total concentration of polymer in the solution (30 mg/mL). The block copolymers employed were PS_{42}-*b*-$PDMAEMA_{50}$, PS_{42}-*b*-$PDMAEMA_{27}$, PS_{42}-*b*-$PDMAEMA_{16}$, PS_{42}-*b*-$PDMAEMA_{7}$ and a quaternized PS_{42}-*b*-$PDMAEMAQ_{16}$. Films were obtained from these solutions by casting onto glass wafers at room temperature under controlled humidity inside of a closed chamber. The samples using blends of the block copolymers were obtained using saturated vapor humidities (> 99% relative humidity (RH)).

In addition, for comparative purposes, a porous surface was prepared using exclusively polystyrene (PS) and chloroform as solvent. This solution was casted under a saturated vapor atmosphere.

Experimental protocol for the cell-adhesion experiments

Prior to cell studies, all surfaces were sterilized with an 80 % ethanol solution rinsing four times during 10 min. Then, the honeycomb surfaces were washed with PBS four times, exposed to UV radiation during 20 min, washed two times with incomplete culture medium (DMEM, D6429; Sigma Aldrich), and finally washed with complete culture medium (FBS and antibiotics) for 30 min.

The cell studies were carried out using C166-GFP, a mouse endothelial cell line (ATCC® CRL-2583™). Routine passaging of the cell line was performed with DMEM high in glucose, supplemented with 10% fetal bovine serum (FBS, Hyclone®, Thermo Scientific) plus antibiotics (100 U/mL penicillin and 100 µg/mL streptomycin sulfate; Sigma Aldrich, St. Louis, MO). The medium was refreshed every 2 or 3 days.

For culturing cells over the porous films, the endothelial cells were seeded on the samples in supplemented DMEM, and the polymers were placed in a non-treated 24-well plate (Corning Costar®) in maintenance medium, incubated at 37°C with 5% CO_2 in a humidified incubator. For experiments on PS-copolymers, cells were seeded at a density of 15×10^3/polymers.

Metabolic activity study: Alamar Blue assay.

Metabolic activity of cells was measured by Alamar Blue assay at 96 h, this was performed following the manufacturer's instructions (Biosource). Assays were performed in triplicate on each sample type. This method is non-toxic, scalable and uses the natural reducing power of living cells, generating a quantitative measure of cell viability and cytotoxicity. Briefly, Alamar Blue dye (10 % of the culture volume) was added to each well, containing living cells seeded over samples, and incubated for 90 min. The fluorescence ($\lambda_{ex}/\lambda_{em}$ 535/590 nm) of each well was measured using a plate-reader (Synergy HT, Brotek).

Actin and Hoechst staining

Actin labeling was performed in order to evaluate qualitatively F-actin microfilaments of cytoskeleton (involved in mobility and intracellular scaffold formation). Additionally, Hoechst staining was carried out to determinate the number of viable cells. Cells on the films were fixed at 96 h with 4% paraformaldehyde (PFA) solution for 10 min. After PFA was removed, cells were rinsed with PBS twice and permeabilized with 0.1% (v/v) Triton X-100. Then, the cells were washed with PBS and stained with Texas Red®-X phalloidin (Life Technologies), a high-affinity F-actin probe conjugated to red fluorochrome, for 20 minutes at room temperature and in darkness, followed by Hoechst staining (Invitrogen, Molecular Probes®). Finally fluorescent-

labeled cells were observed using an inverted fluorescence microscope (Olympus IX51) with a TRICT filter ($\lambda_{ex}/\lambda_{em}$=550/600 nm) for Actin and DAPI filter for Hoechst ($\lambda_{ex}/\lambda_{em}$ = 380/455 nm) using CellD analysis software (Olympus).

Bacterial adhesion and live/die assays

Staphylococcus aureus strain RN4220 carrying the plasmid pCN57 for green fluorescent protein (GFP) expression was grown overnight at 37°C in Luria–Bertani (LB) media with erythromycin (10 μg mL^{-1}). The cells were centrifuged and washed three times in saline buffer (150 mM NaCl). The solution was adjusted to a cell concentration that corresponds to an optical density (OD) at 600 nm of 1.0 checked using a NanoDrop One (Termofisher).

The different patterned polymeric surfaces were incubated for 1 hour with a bacterial suspension at OD = 1.0. After incubation the surfaces were washed with saline buffer three times for 15 minutes. Bacterial adhesion was monitored by fluorescence microscopy using a Leica DMI-6000 fluorescence microscope. Images were acquired using x63 magnification and the corresponding filter set for imaging green fluorescence corresponding to the GFP expressed in the bacteria.

After adhesion, the bacteria viability was measured using Propidium iodine staining, as indicated in the LIVE/DEAD BacLight Bacterial Viability Kit. Propidium iodine is a red-fluorescent nucleic acid stain that penetrates only cells with disrupted membranes and intercalates DNA. The different surfaces with attached bacteria were incubated with propidium iodide (5 mg mL^{-1}) for 15 minutes, followed by rinsing with saline solution (10 times). Phase contrast, green and red fluorescence microscopy images were taken at x63 magnification. The bacterial cell density and the viability were quantified using ImageJ.

Results and discussion

Strategy to develop selective antibacterial surfaces

The concept of the fabrication of functional surfaces with selective antimicrobial activity is depicted in **Figure 1**. Whereas the sizes of bacteria are in range of 1 up to 5 µm (for this study we employed *S. aureus* with 1µm diameter) typically mammalian cells are several times larger (between 10 and 20 µm). As a result, providing functional surfaces with pores between these values (for instance between 4-6 µm) may limit the interaction of the cells with the inner part of the pores while, according to previous findings[39], bacteria may enter inside of the cavities. Provided that antimicrobial functional groups are selectively located at the pore surface the effect of the antimicrobial groups will affect, upon contact, only bacteria. This strategy is expected to permit the design of functional surfaces for the growth of mammalian cells with antibacterial activity and reduced the side effects due to the limited interactions between the antimicrobial functional groups and the cell wall.

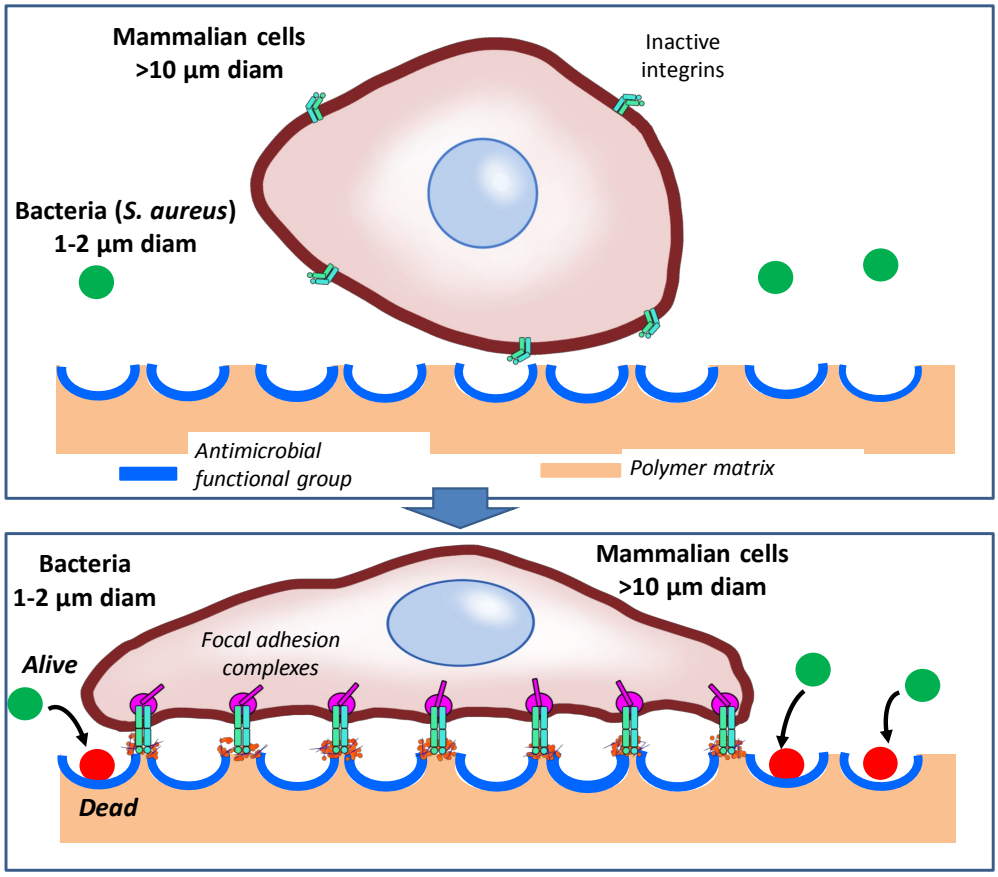

Figure 1. Illustration of the strategy proposed to fabricate functional porous surface selective against bacteria. Mammalian cells interacts only with the inner part of the pores, and through

integrin activation, focal adhesion complexes are stablished. In contrast, bacteria may enter inside of the cavities and be affected by antimicrobial functional groups.

The porous films selected for this study were prepared using polymer blends comprising a PS-*b*-PDMAEMA or PS-*b*-PDMAEMAQ block copolymers and high molecular polystyrene as a matrix. The PS-*b*-PDMAEMA block copolymer employed was synthesized by ATRP in two consecutive polymerization steps following previously reported procedures[40]. ATRP allows among others a precise control over the chemical structure providing block copolymers with narrow polydispersities (PD:1.2-1.3) as well as variable chemical composition. For this study, the block copolymers PS_{42}-*b*-$PDMAEMA_{50}$, PS_{42}-*b*-$PDMAEMA_{27}$, PS_{42}-*b*-$PDMAEMA_{16}$, PS_{42}-*b*-$PDMAEMA_{7}$ were prepared. Moreover, in a following step, the diblock copolymers were quaternized to provide quaternary ammonium salt groups. It is worth mentioning that these positively charged groups are known for their excellent antimicrobial properties[4]. For this part of the study the block copolymer PS_{42}-*b*-$PDMAEMA_{16}$ was selected. The ^{1}H-NMR spectra (Supplementary information-Figure S1) clearly indicated that upon treatment with CH_3I, the dimethylamino groups were quantitatively quaternized. In particular, the ^{1}H-NMR signals assigned to the methyl groups appearing at 2.3 ppm in PDMAEMA clearly shifted to 3.3 ppm upon quaternization. Equally, the signal associated the $-C\underline{H}_2$-$N(CH_2)_2$ could be observed at 2.6 ppm in the non-quaternized PDMAEMA and also shifts upon quaternization to 3.9 ppm.

Fabrication of microporous surfaces from block copolymer/homopolymer blends

The amphiphilic block copolymers (PS_{42}-*b*-$PDMAEMA_{50}$, PS_{42}-*b*-$PDMAEMA_{27}$, PS_{42}-*b*-$PDMAEMA_{16}$ and PS_{42}-*b*-$PDMAEMA_{7}$) were used as additives for the fabrication of porous surfaces by using the Breath Figures approach. In order to achieve the appropriate pore size and a homogeneous surface pore distribution several parameters were explored. It is already widely accepted that pore size and distribution of films prepared using the Breath Figures approach directly depend on several parameters including the relative humidity, the polymer concentration and in the case of blends the relative amount of the components.

In order to produce microporous surfaces with pore diameters in the range of 3-7 μm (i.e. above the diameter of the bacteria employed and below the cell size), the first aspect explored was the relative humidity (data not shown). According to our findings[41] and other previously reported examples[12] a rather large humidity is required to induce the pore formation. In particular, we evidenced that a relative humidity above 95% produced optimal results in the explored system. Lower relative humidities led to poor condensation and therefore scarce pore formation (supporting information Figure S5).

Another interesting parameter to vary the pore dimensions, when employing amphiphilic block copolymers as a blend component, is related to the hydrophilic/hydrophobic ratio of the block copolymer, *i.e.* the length of the hydrophilic block in comparison to the hydrophobic block. To analyze the role of this parameter, four different block copolymers were employed maintaining the humidity (95% r.h.), the blend composition (80 wt% homopolymer and 20 wt% block copolymer) as well as the polymer concentration (30 mg/mL) constant. As depicted in **Figure 2**, block copolymers with rather large PDMAEMA chain lengths produced poorly ordered porous surfaces. Most probably, based in previous findings using amphiphilic copolymers, [42] the chemical composition of the block copolymer with a large hydrophilic block is not able to prevent the coagulation of the water droplets. On the contrary, by using block copolymers with a shorter hydrophilic PDMAEMA block favors the formation of well-ordered porous surfaces with pores ranging between 5-6 μm.

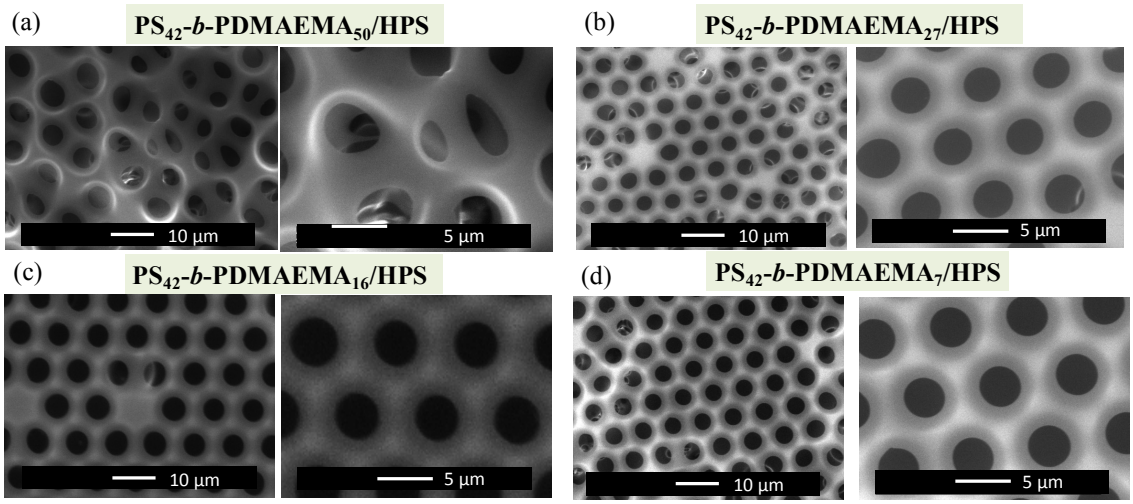

Figure 2. Scanning microscope images of the porous films fabricated using blends of 20 wt% of the different diblock copolymers and 80 wt% high molecular weight PS. The images correspond to the following blends (a) PS_{42}-*b*-$PDMAEMA_{50}$/PS (b) PS_{42}-*b*-$PDMAEMA_{27}$/PS (c) PS_{42}-*b*-$PDMAEMA_{16}$/PS and (d) PS_{42}-*b*-$PDMAEMA_{7}$/PS. The total polymer concentration was set to at 30 mg/mL for this experiment and the relative humidity above 95%.

Prior to analyzing the cell and bacterial interactions with these films, the role of the polymer concentration was equally investigated. In **Figure 3** are shown the scanning microscopy images of the porous films prepared using two different diblock copolymer/homopolymer (DBC/PS) blends charged either with 10 or 20 % in DBC and thus, 80 or 90 % in PS. The porous films have been prepared, in addition at three different concentrations ranging from 5 up to 30 mg/mL. Within this range of concentrations a clear tendency was observed in which a random and rather heterogeneous in size (2-10 μm) distributed porous surfaces are formed at concentrations around 5 mg/mL, while an increase in the polymer concentration up to 10 mg/mL or even to 30 mg/mL significantly improves the order of the porous surface. In addition to the order and homogeneous pore size, it is interesting to note that those films prepared with a higher amount of block copolymer are expected to have a larger amount of PDMAEMA and in turn, as will be depicted, a larger amount of antimicrobial PDMAEMAQ inside of the pores.

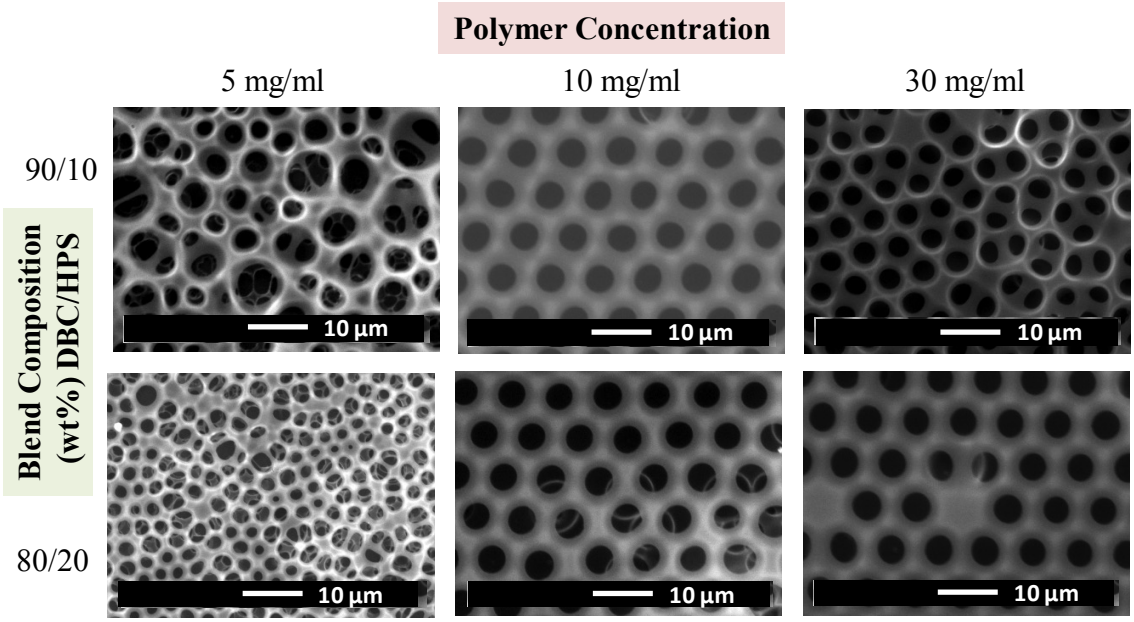

Figure 3. Scanning microscope images of the porous films fabricated using blends either 80 wt% or 90 wt% of PS_{42}-*b*-$PDMAEMA_{16}$ diblock copolymer (DBC) and either 20 wt% or 10 wt% of high molecular weight PS (PS). The total polymer concentration was set to at 30 mg/mL for this experiment.

Based on this finding, the block copolymer with the composition PS_{42}-*b*-$PDMAEMA_{16}$ has been selected as illustrative example for its quaternization and analysis of the antimicrobial properties. Equally, the relative humidity and polymer concentration were fixed to 95% and 30mg/mL for the rest of the experiments. More precisely, the composition of the samples prepared is summarized in **Table 1**.

Table 1. Composition (wt%) of the porous films prepared and evaluated as selective antimicrobial surfaces

	PS (wt%)	PS_{42}-*b*-$PDMAEMA_{16}$ (wt%)	PS_{42}-*b*-$PDMAEMAQ_{16}$ (wt%)
PS	100	0	0
PSD305	95	5	0
PSD31	90	10	0
PSD32	80	20	0
PSDQ305	95	0	5
PSDQ31	90	0	10
PSDQ32	80	0	20

Analysis of the surface structure evidenced only slight differences between the pore size and distribution between the samples prepared using either 10 or 20 wt% of block copolymer quaternized and non-quaternized. Interestingly, in both cases the pore sizes observed did not

vary significantly by increasing the block copolymer content. On the contrary, the sample prepared using 5 wt% of non-quaternized block copolymer presented an ordered array of pores while the quaternized leads to larger pore sizes and broader size distributions. Nevertheless the pore sizes remains significantly below the diameter of mammalian cells which maybe a crucial aspect in the antimicrobial performance. For this reason, all the systems were explored both in view of the biocompatibility towards mammalian cells and their antimicrobial activity against bacteria.

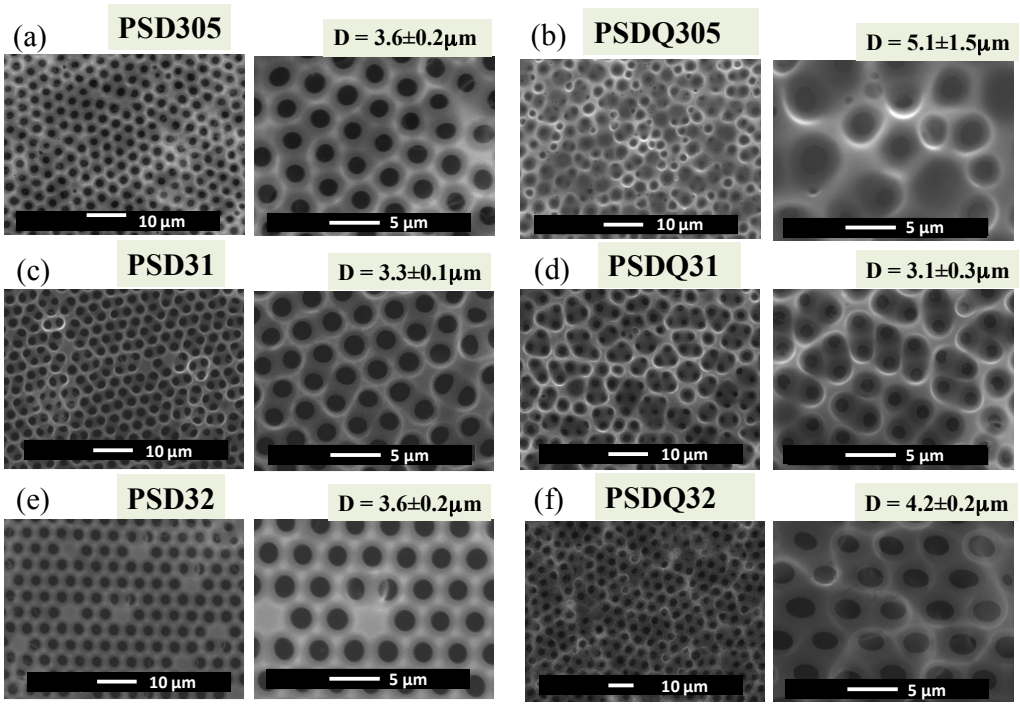

Figure 4. Comparison of the porous films obtained using either the non-quaternized or the quaternized PS_{42}-*b*-$PDMAEMA_{16}$ diblock copolymer. The concentration of block copolymer in the blend was varied: (a) - (b) 5 wt% (PSD305 and PSDQ305), (c) - (d) 10 wt% (PSD31 and PSDQ31) and (e)-(f) 20 wt% (PSD32 and PSDQ32). Q stands for quaternized (correspond to the right column images). The total polymer concentration was set to at 30 mg/mL for this experiment. The average diameters of the pores and the standard errors are shown in µm.

In addition to the appropriate pore size the strategy proposed requires a precise localization of the antimicrobial functional groups inside of the pores. Confocal Raman was employed in order to investigate the chemical composition enabling to distinguish between the two regions pore wall and the surface. By considering the Raman spectra of the pure components, *i.e.* polystyrene and the diblock copolymer (see Supporting information – **Figure S3**) we evidenced several differences but probably the most clear is the signal at 2789 cm^{-1} present exclusively in PDMAEMA. In **Figure 5(d)** are depicted the confocal Raman spectra of the resulting films obtained both in the pore wall and at the surface of the film. The exact location in which the spectra have been obtained is indicated in **Figure 5(b)** by a cross. Interestingly, the signal can only be observed in those spectra obtained inside the pores indicating a selective enrichment of the diblock copolymer in this particular area. As expected and in agreement with the observations of other groups[43-45] during the pore formation the hydrophilic groups of the diblock copolymer are able to rearrange around the pore surface. This particular orientation is fixed when the solvent and the water droplet evaporate thus finally leading to a non-uniform surface chemical composition but a localized positioning of the diblock copolymer. This effect can be clearly observed by mapping the surface composition in the same cross-sectional profile (**Figure 5(c)**). While the red color indicates the presence exclusively of polystyrene, the violet color observed inside the pore indicates variations in the chemical composition provided by the block copolymer.

In addition to the polymer porous films obtained using the non-quaternized block copolymer, similar confocal Raman analysis were carried out on those films prepared using the quaternized block copolymer. As depicted in **Figure 6(a)** several distinct signals can be observed in the block copolymer that will serve to identify the position of the block copolymer at the polymer surface. As a result, by comparison of the signals representative of polystyrene (*i.e.* 1009 cm^{-1}) and the carbonyl band of the diblock copolymer at 1734 cm^{-1} it is possible to construct a map with the variable composition at the surface. In **Figure 6(c)** is represented the composition focusing in one single pore that, similarly to the films prepared using the non-quaternized block

copolymers, presented an enrichment of the block copolymer inside the pore, while the rest of the surface is mainly formed by PS.

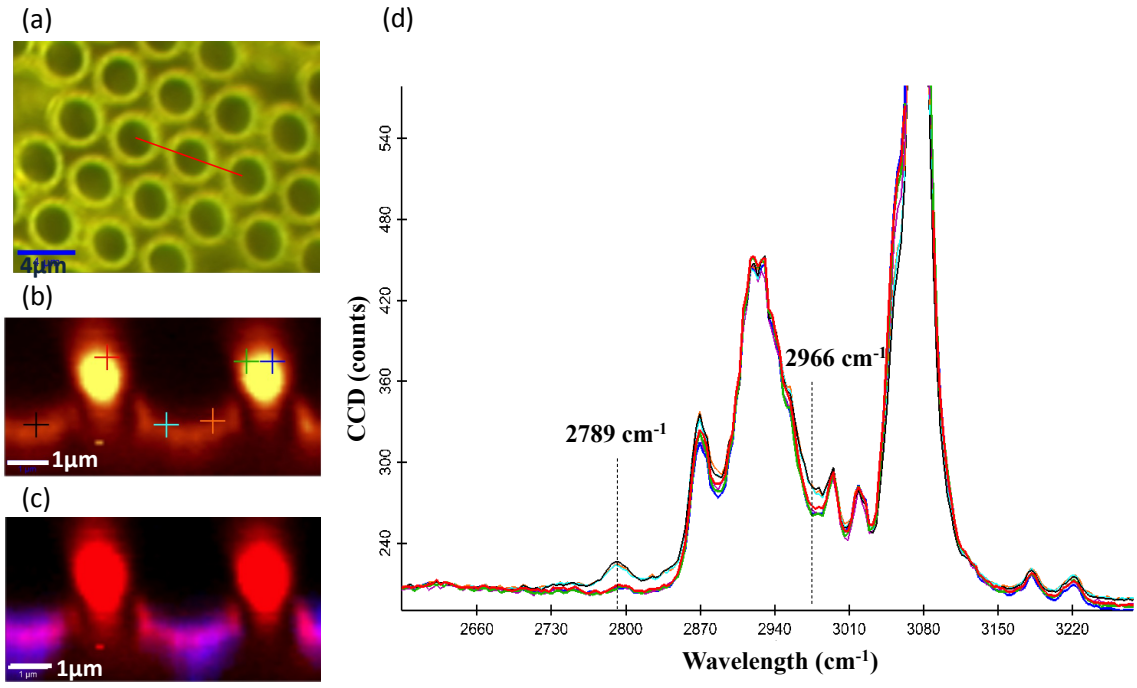

Figure 5. Raman Confocal analysis of a porous film prepared using the non-quaternized PS_{42}-*b*-$PDMAEMA_{16}$ diblock copolymer 20 wt % and PS (Sample: PSD32). (a) Optical image of the porous surface (b) Cross-sectional profile marked with crosses indicating the position in which the raman of (d) have been measured. (c) Cross-sectional profile to identify variations of the chemical composition inside the pores (violet) formed mainly by the diblock copolymer and outside the pores (red) indicating the presence of polystyrene.

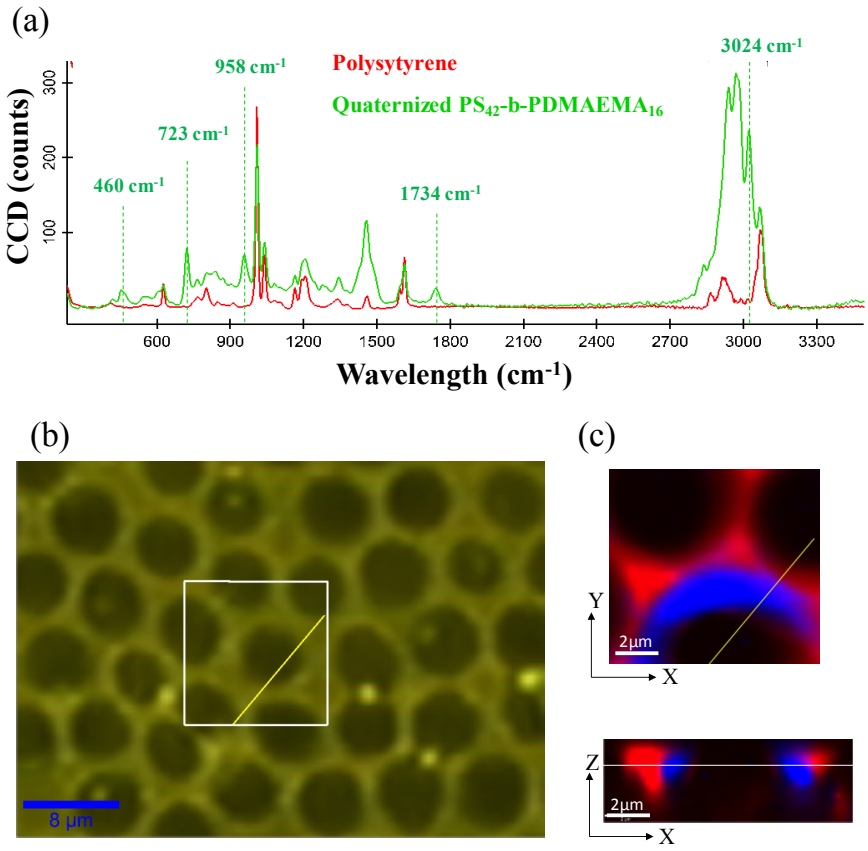

Figure 6. Comparison of the porous films obtained using quaternized PS_{42}-*b*-$PDMAEMAQ_{16}$ diblock copolymer (20 wt%) and PS (80%). (Sample: PSDQ32). (a) Raman spectra of the blend components, *i.e.* polystyrene and the quaternized block copolymer. (b) Optical image of the porous surface and (c) cross-sectional profiles in the Y-X axis (above) and in the Z-X axis indicanting the presence of quaternized block copolymer inside the pores.

The porous samples with different compositions, including the control surface PS and surfaces with different concentrations of the PS_{42}-*b*-$PDMAEMA_{16}$ diblock copolymer (5, 10, and 20 % for PSD305, PSD31, and PSD32, respectively) and their corresponding quaternized variants (PSDQ305, PSDQ31, PSDQ32) were evaluated with the endothelial cell line (C166-GFP) in order to assess their biocompatibility in a mammalian cell model. At 96 h, cell metabolic activity was measured (**Figure S4**), showing that all samples were cytocompatible.

PSD32 surface, which has a major % of copolymer, showed a less expanded morphology (**Figure 7f**) and a lower metabolic activity measure (**Figure S4**) in comparison with PSD31 and PSD305. These two surfaces presented a similar metabolic activity and a proper monolayer formation. In contrast, quaternized variants exhibited a diminished cell support capacity with lower metabolic activity values. However, general cell viability was not affected and similar trends between samples were detected. PSDQ305 and PSDQ31 displayed a well-grown monolayer whereas cells proliferating over PSDQ32 showed a less expanded phenotype, with a rounded morphology and the lowest metabolic activity reading (**Figure 7** and **S4**).

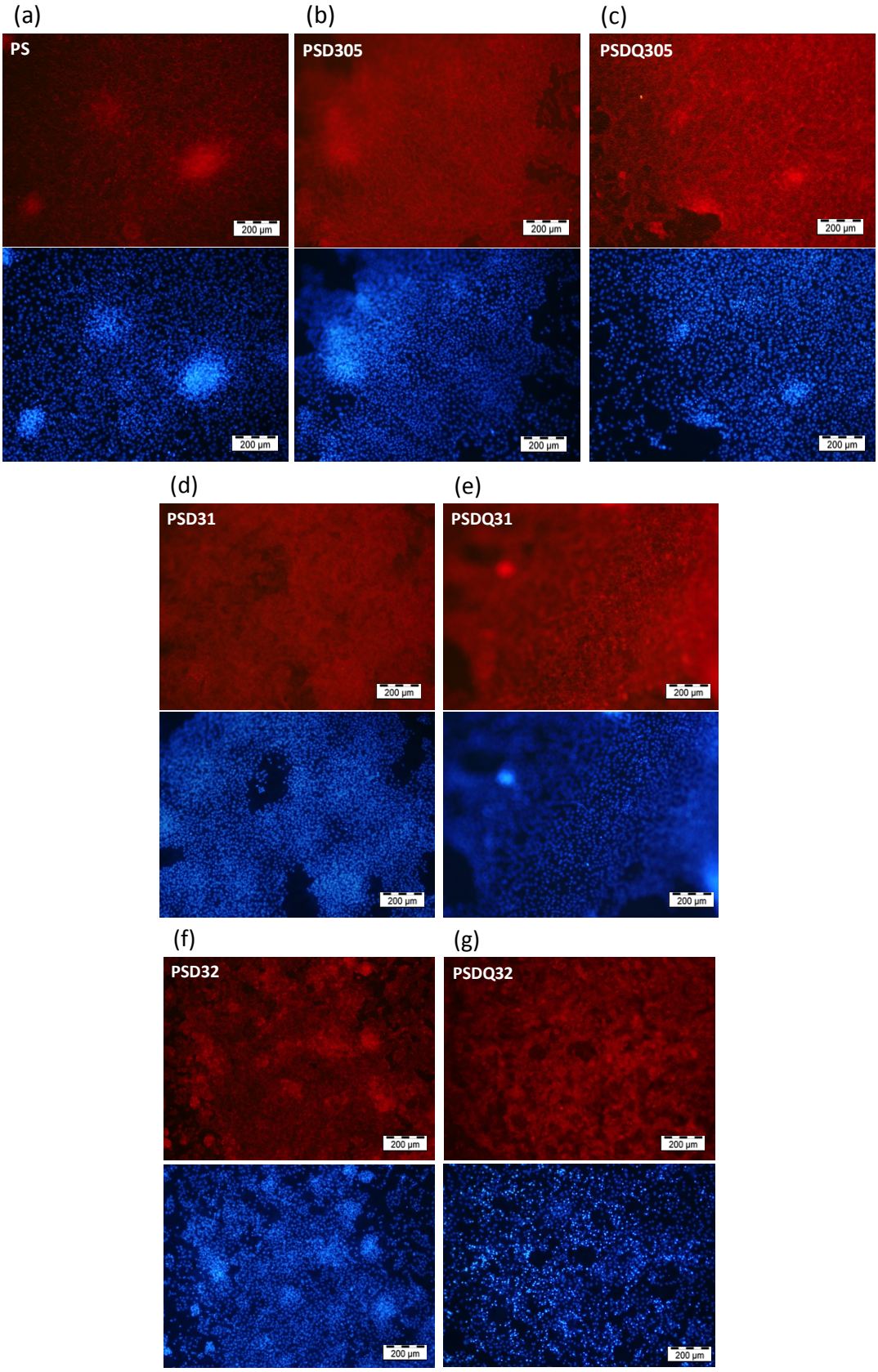

Figure 7. Actin staining (red), and Hoechst (blue), respectively, after fixation at 96 h of culture: (a) PS (b), PSD305 (c) PSDQ305, (d) PSD31, (e) PSDQ31, (f) PSD32 and (g) PSDQ32.

Bacterial assays

The porous surfaces with different compositions, including the control surface PS and surfaces with different concentrations of the PS_{42}-*b*-$PDMAEMA_{16}$ diblock copolymer (5, 10, and 20 wt % for PSD305, PSD31, and PSD32, respectively) and their corresponding quaternized variants PSDQ305, PSDQ31, PSDQ32 were tested for their bacterial adhesion and bactericidal properties. In these experiments *S. aureus* is used as a model bacteria since it is well-known its ability to become resistant to antibiotics resulting for example in the Methicillin-*resistant S. aureus* (MRSA) responsible of many hospital-acquired infections. After incubation of the surfaces with standarized solutions of bacteria expressing a fluorescent proteins the surfaces were washed and imaged in order to determine the amount of bacteria on the surfaces (**Figure 8**). As can be observed from the images and from the quantification of the number of bacteria per surface area (**Table 2**) the bacteria adhesion upon one hour incubation was very similar on the different surfaces, independently of their composition.

Table 2. Quantification of adhesion of the bacteria to the different surfaces

Sample	Adhesion (number of bacteria/cm^2)
PS	6.63E+07 ± 5.69E+06
PSD305	1.19E+08 ± 2.02E+06
PSD31	7.56E+07 ± 4.57E+06
PSD32	7.34E+07 ± 7.37E+06
PSDQ305	6.75E+07 ± 3.47E+06
PSDQ31	7.88E+07 ± 8.89E+06
PSDQ32	6.78E+07 ± 7.16E+06

Since the adhesion properties of the different surfaces were similar, it is interesting to test the potential bactericidal effect of the presence of antibacterial functionalities in the pores. Surfaces

with different percentages of quaternized and non-quaternized PDMAEMA were tested at different times upon adhesion. The surfaces with the adhered bacteria were incubated with propidium iodide, a membrane impermeant dye that stains dead bacteria after adhesion, 24 h and 48 h after adhesion. Fluorescent images are acquired in order to calculate the ratio between live and dead bacteria under each experimental condition (**Figure 8**).

As expected the PS control simple did not show any bactericidal activity over time. The non-quaternized polymers (PSD series) showed very weak bactericidal activity at the highest percentage of PDMAEMA (20 %) and after 48 hours incubation time. However, the quaternized porous surfaces showed a significant bactericidal activity. In **Figure 9** can be observed a clear trend in the effect of the increase percentage of quaternized PDMAEMA and the incubation time on the bacterial survival. For lower percentages of PDMAEMA (5 wt% in PSDQ305) a noticeable effect is detected only after 48 h, contrary for the highest concentration (20 wt% of PDMAEMA in PSDQ32) a bactericidal effect was detected right after the adhesion experiment (0 h time). In addition a quantification of the fluorescence microscopy images performed using Image J. The quantitative results shown in **Figure 9** fully support the trends observed in the images. In conclusion, the designed porous surfaces with specific quaternized antibacterial functional groups in the pores present an efficient bactericidal activity.

Thus, the described functional microporous surfaces presented excellent antimicrobial properties when the polymer is in its quaternized form. Interestingly, quaternary ammonium groups, which have been reported in several studies to have a reduced biocompatibility,[33-34] are in this design, hidden from the cell contact. As a result, the materials developed presented simultaneously high biocompatibility towards mammalian cells and antimicrobial activity against *S. aureus*.

It is worth mentioning that, as shown in Figure 8, died bacteria appeared in any position independently of the surface chemistry. To the best of our knowledge this may be due to the dynamic diffusion in and out of the pores, i.e. living bacteria diffuse into the pores where they are effectively killed and diffuse out of the pores.

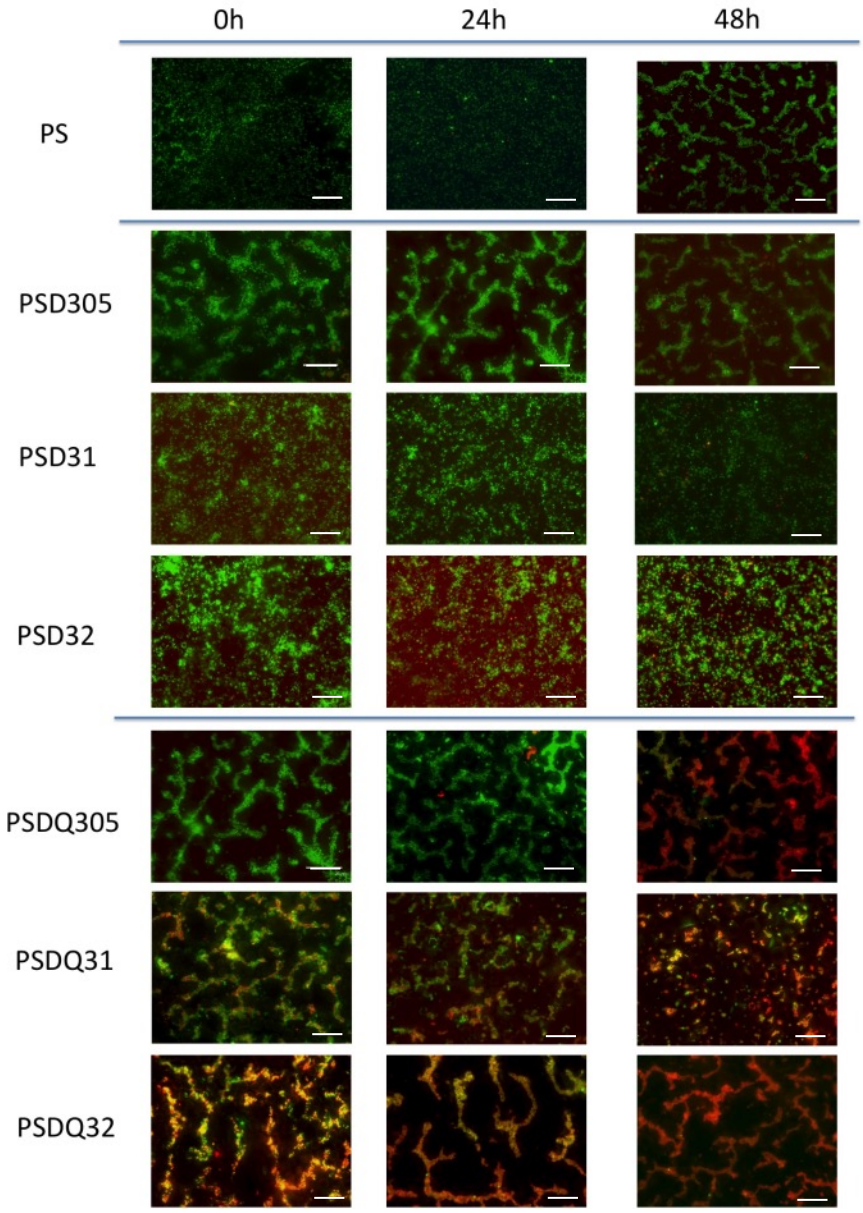

Figure 8. Bactericidal activity of the porous polymeric surfaces. Fluorescence microscopy images of the polymeric surfaces incubated with *S. aureus* labeled with Green fluorescent protein and stained with propidium iodide. Images were acquired using the green and red channels at 63 x magnification. For each polymeric surface overlay images of the two channels are generated using Image J. The scale bars correspond to 20 μm.

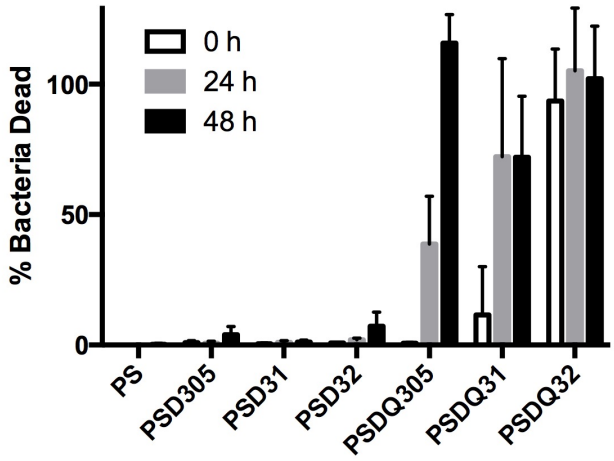

Figure 9. Quantification of the % of bacteria dead for each experimental condition. The quantification was performed by counting the number of cells stained in red or in green using Image J.

Conclusions

In this manuscript the fabrication of effective antimicrobial surfaces based on the functionalization of porous films obtained by the Breath Figures approach has been reported. By blending two different polymers, herein polystyrene and an amphiphilic diblock copolymer (PS-*b*-PDMAEMA and PS-*b*-PDMAEMAQ) micrometer size porous surfaces were obtained in a single step. More interestingly, studies about the chemical distribution evidenced that far from being homogeneous the diblock copolymer has a large tendency to rearrange and enrich the pore surface while the rest of the surface is depleted from the diblock copolymer. This distribution allowed us to selectively localize the antimicrobial moieties in the micrometer size cavities only accessible to the bacteria. As a result, the latter are readily killed. On the contrary, mammalian cells, significantly larger in size do not come in contact with the antimicrobial groups and are able to grow and proliferate on these surfaces.

This strategy opens new alternatives for the preparation of multiple materials and devices, in particular for biorelated purposes.

Acknowledgments

The authors gratefully acknowledge support from the Consejo Superior de Investigaciones Científicas (CSIC). Equally, this work was financially supported by the Ministerio de Economía y Competitividad (MINECO) through MAT2016-78437-R (JRH), BIO2012-34835 and BIO2016- 77367 (ALC).

References

(1. Saginur, R.; StDenis, M.; Ferris, W.; Aaron, S. D.; Chan, F.; Lee, C.; Ramotar, K., Multiple Combination Bactericidal Testing of Staphylococcal Biofilms from Implant-Associated Infections. *Antimicrobial Agents and Chemotherapy* **2006,** *50* (1), 55-61.
2. Zimmerli, W.; Trampuz, A., Implant-associated infection. In *Biofilm Infections*, Springer: **2011**, pp 69-90.
3. Hetrick, E. M.; Schoenfisch, M. H., Reducing implant-related infections: active release strategies. *Chemical Society Reviews* **2006,** *35* (9), 780-789.
4. Kenawy, E.-R.; Worley, S. D.; Broughton, R., The Chemistry and Applications of Antimicrobial Polymers: A State-of-the-Art Review. *Biomacromolecules* **2007,** *8* (5), 1359-1384.
5. Munoz-Bonilla, A.; Cerrada, M. L.; Fernandez-Garcia, M., CHAPTER 1 Introduction to Antimicrobial Polymeric Materials. In *Polymeric Materials with Antimicrobial Activity: From Synthesis to Applications*, The Royal Society of Chemistry: **2014**, pp 1-21.
6. Siedenbiedel, F.; Tiller, J. C., Antimicrobial Polymers in Solution and on Surfaces: Overview and Functional Principles. *Polymers* **2012,** *4* (1), 46-71.
7. Manabe, K.; Nishizawa, S.; Shiratori, S., Porous Surface Structure Fabricated by Breath Figures that Suppresses Pseudomonas aeruginosa Biofilm Formation. *ACS Applied Materials & Interfaces* **2013,** *5* (22), 11900-11905.
8. Yu, Q.; Wu, Z.; Chen, H., Dual-function antibacterial surfaces for biomedical applications. *Acta biomaterialia* **2015,** *16*, 1-13.
9. Séon, L.; Lavalle, P.; Schaaf, P.; Boulmedais, F., Polyelectrolyte multilayers: a versatile tool for preparing antimicrobial coatings. *Langmuir* **2015,** *31* (47), 12856-12872.
10. Cloutier, M.; Mantovani, D.; Rosei, F., Antibacterial coatings: challenges, perspectives, and opportunities. *Trends in biotechnology* **2015,** *33* (11), 637-652.
11. Raphel, J.; Holodniy, M.; Goodman, S. B.; Heilshorn, S. C., Multifunctional coatings to simultaneously promote osseointegration and prevent infection of orthopaedic implants. *Biomaterials* **2016,** *84*, 301-314.
12. Escale, P.; Rubatat, L.; Billon, L.; Save, M., Recent advances in honeycomb-structured porous polymer films prepared via breath figures. *European Polymer Journal* **2012,** *48* (6), 1001-1025.
13. de León, A. S.; del Campo, A.; Fernández-García, M.; Rodríguez-Hernández, J.; Muñoz-Bonilla, A., Hierarchically Structured Multifunctional Porous Interfaces through Water Templated Self-Assembly of Ternary Systems. *Langmuir* **2012,** *28* (25), 9778-9787.
14. Stenzel, M. H.; Barner-Kowollik, C.; Davis, T. P., Formation of honeycomb-structured, porous films via breath figures with different polymer architectures. *Journal of Polymer Science Part A: Polymer Chemistry* **2006,** *44* (8), 2363-2375.

15. Nishikawa, T.; Ookura, R.; Nishida, J.; Arai, K.; Hayashi, J.; Kurono, N.; Sawadaishi, T.; Hara, M.; Shimomura, M., Fabrication of honeycomb film of an amphiphilic copolymer at the air−water interface. *Langmuir* **2002,** *18* (15), 5734-5740.
16. Tsuruma, A.; Tanaka, M.; Yamamoto, S.; Shimomura, M., Control of neural stem cell differentiation on honeycomb films. *Colloids and Surfaces A: Physicochemical and Engineering Aspects* **2008,** *313-314*, 536-540.
17. Sanz de Leon, A.; Rodriguez-Hernandez, J.; Cortajarena, A. L., Honeycomb patterned surfaces functionalized with polypeptide sequences for recognition and selective bacterial adhesion. *Biomaterials* **2013,** *34* (5), 1453-1460.
18. Nishida, J.; Nishikawa, K.; Nishimura, S.-I.; Wada, S.; Karino, T.; Nishikawa, T.; Ijiro, K.; Shimomura, M., Preparation of self-organized micro-patterned polymer films having cell adhesive ligands. *Polymer Journal* **2002,** *34* (3), 166-174.
19. Tanaka, M.; Takebayashi, M.; Miyama, M.; Nishida, J.; Shimomura, M., Design of novel biointerfaces (II). Fabrication of self-organized porous polymer film with highly uniform pores. *Bio-Medical Materials and Engineering* **2004,** *14* (4), 439-446.
20. Tanaka, M.; Nishikawa, K.; Okubo, H.; Kamachi, H.; Kawai, T.; Matsushita, M.; Todo, S.; Shimomura, M., Control of hepatocyte adhesion and function on self-organized honeycomb-patterned polymer film. *Colloids and Surfaces A: Physicochemical and Engineering Aspects* **2006,** *284-285*, 464-469.
21. Tanaka, M.; Takayama, A.; Ito, E.; Sunami, H.; Yamamoto, S.; Shimomura, M., Effect of pore size of self-organized honeycomb-patterned polymer films on spreading, focal adhesion, proliferation, and function of endothelial cells. *Journal of Nanoscience and Nanotechnology* **2007,** *7* (3), 763-772.
22. Sato, T.; Tanaka, M.; Yamamoto, S.; Ito, E.; Shimizu, K.; Igarashi, Y.; Shimomura, M.; Inokuchi, J.-i., Effect of honeycomb-patterned surface topography on the function of mesenteric adipocytes. *Journal of Biomaterials Science, Polymer Edition* **2010,** *21*, 1947-1956.
23. Tsuruma, A.; Tanaka, M.; Fukushima, N.; Shimomura, M., Morphological changes in neurons by self-organized patterned films. *e-Journal of Surface Science and Nanotechnology* **2005,** *3*.
24. Wu, X.; Wang, S., Regulating MC3T3-E1 Cells on Deformable Poly(epsilon-caprolactone) Honeycomb Films Prepared Using a Surfactant-Free Breath Figure Method in a Water-Miscible Solvent. *Acs Applied Materials & Interfaces* **2012,** *4* (9), 4966-4975.
25. Yamamoto, S.; Tanaka, M.; Sunami, H.; Ito, E.; Yamashita, S.; Morita, Y.; Shimomura, M., Effect of honeycomb-patterned surface topography on the adhesion and signal transduction of porcine aortic endothelial cells. *Langmuir* **2007,** *23* (15), 8114-8120.
26. Du, M.; Zhu, P.; Yan, X.; Su, Y.; Song, W.; Li, J., Honeycomb self-assembled peptide scaffolds by the breath figure method. *Chemistry - A European Journal* **2011,** *17* (15), 4238-4245.
27. Beattie, D.; Wong, K. H.; Williams, C.; Poole-Warren, L. A.; Davis, T. P.; Barner-Kowollik, C.; Stenzel, M. H., Honeycomb-structured porous films from polypyrrole-containing block copolymers prepared via RAFT polymerization as a scaffold for cell growth. *Biomacromolecules* **2006,** *7* (4), 1072-1082.
28. Duan, S.; Yang, X.; Mao, J.; Qi, B.; Cai, Q.; Shen, H.; Yang, F.; Deng, X.; Wang, S., Osteocompatibility evaluation of poly(glycine ethyl ester-co-alanine ethyl ester)phosphazene with honeycomb-patterned surface topography. *Journal of Biomedical Materials Research Part A* **2013,** *101A* (2), 307-317.
29. Fukuhira, Y.; Ito, M.; Kaneko, H.; Sumi, Y.; Tanaka, M.; Yamamoto, S.; Shimomura, M., Prevention of postoperative adhesions by a novel honeycomb-patterned poly(lactide) film in a rat experimental model. *Journal of Biomedical Materials Research Part B-Applied Biomaterials* **2008,** *86B* (2), 353-359.

30. Jiang, X.; Zhang, T.; He, S.; Ling, J.; Gu, N.; Zhang, Y.; Zhou, X.; Wang, X.; Cheng, L., Bacterial Adhesion on Honeycomb-Structured Poly(L-Lactic Acid) Surface with Ag Nanoparticles. *Journal of Biomedical Nanotechnology* **2012,** *8* (5), 791-799.
31. Yamamoto, S.; Tanaka, M.; Sunami, H.; Arai, K.; Takayama, A.; Yamashita, S.; Morita, Y.; Shimomura, M., Relationship between adsorbed fibronectin and cell adhesion on a honeycomb-patterned film. *Surface Science* **2006,** *600* (18), 3785-3791.
32. Nishikawa, T.; Nishida, J.; Ookura, R.; Nishimura, S.-I.; Wada, S.; Karino, T.; Shimomura, M., Honeycomb-patterned thin films of amphiphilic polymers as cell culture substrates. *Materials Science and Engineering: C* **1999,** *8–9*, 495-500.
33. Xue, Y.; Xiao, H.; Zhang, Y., Antimicrobial Polymeric Materials with Quaternary Ammonium and Phosphonium Salts. *International Journal of Molecular Sciences* **2015,** *16* (2), 3626-3655.
34. Dutta, P.; Dey, J.; Shome, A.; Das, P. K., Nanostructure formation in aqueous solution of amphiphilic copolymers of 2-(N,N-dimethylaminoethyl)methacrylate and alkylacrylate: Characterization, antimicrobial activity, DNA binding, and cytotoxicity studies. *International Journal of Pharmaceutics* **2011,** *414* (1), 298-311.
35. Álvarez-Paino, M.; Muñoz-Bonilla, A.; López-Fabal, F.; Gómez-Garcés, J. L.; Heuts, J. P. A.; Fernández-García, M., Effect of glycounits on the antimicrobial properties and toxicity behavior of polymers based on quaternized DMAEMA. *Biomacromolecules* **2015,** *16* (1), 295-303.
36. Wu, B.-H.; Zhu, L.-W.; Ou, Y.; Tang, W.; Wan, L.-S.; Xu, Z.-K., Systematic investigation on the formation of honeycomb-patterned porous films from amphiphilic block copolymers. *The Journal of Physical Chemistry C* **2015,** *119* (4), 1971-1979.
37. Ke, B.-B.; Wan, L.-S.; Li, Y.; Xu, M.-Y.; Xu, Z.-K., Selective layer-by-layer self-assembly on patterned porous films modulated by Cassie–Wenzel transition. *Physical Chemistry Chemical Physics* **2011,** *13* (11), 4881-4887.
38. Ke, B.-B.; Wan, L.-S.; Chen, P.-C.; Zhang, L.-Y.; Xu, Z.-K., Tunable assembly of nanoparticles on patterned porous film. *Langmuir* **2010,** *26* (20), 15982-15988.
39. de León, A. S.; del Campo, A.; Cortajarena, A. L.; Fernández-García, M.; Muñoz-Bonilla, A.; Rodríguez-Hernández, J., Formation of Multigradient Porous Surfaces for Selective Bacterial Entrapment. *Biomacromolecules* **2014,** *15* (9), 3338-3348.
40. Vargas-Alfredo, N.; Rodríguez Hernández, J., Microstructured Polymer Blend Surfaces Produced by Spraying Functional Copolymers and Their Blends. *Materials* **2016,** *9* (6), 431.
41. Muñoz-Bonilla, A.; Fernández-García, M.; Rodríguez-Hernández, J., Towards hierarchically ordered functional porous polymeric surfaces prepared by the breath figures approach. *Progress in Polymer Science* **2014,** *39* (3), 510-554.
42. Bunz, U. H. F., Breath figures as a dynamic templating method for polymers and nanomaterials. *Advanced Materials* **2006,** *18* (8), 973-989.
43. Stenzel, M. H.; Barner‐Kowollik, C.; Davis, T. P., Formation of honeycomb‐structured, porous films via breath figures with different polymer architectures. *Journal of Polymer Science Part A: Polymer Chemistry* **2006,** *44* (8), 2363-2375.
44. Hernández-Guerrero, M.; Stenzel, M. H., Honeycomb structured polymer films via breath figures. *Polymer Chemistry* **2012,** *3* (3), 563-577.
45. Bai, H.; Du, C.; Zhang, A.; Li, L., Breath figure arrays: unconventional fabrications, functionalizations, and applications. *Angewandte Chemie International Edition* **2013,** *52* (47), 12240-12255.

TOC

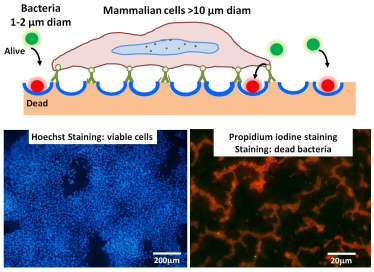
Bacteria
1-2 µm diam
Mammalian cells >10 µm diam
Alive
Dead
Hoechst Staining: viable cells
Propidium iodine staining
Staining: dead bacteria
200µm
20µm